



Textile sludge–sawdust chemically produced activated carbon: equilibrium and dynamics studies of malachite green adsorption

Tang Shu Hui^{1,2} · Muhammad Abbas Ahmad Zaini^{1,2}

Received: 28 March 2020 / Revised: 3 August 2020 / Accepted: 10 August 2020 / Published online: 18 August 2020
© Springer-Verlag GmbH Germany, part of Springer Nature 2020

Abstract

Textile sludge–sawdust chemically produced activated carbon (SSAC) was used in equilibrium and dynamics adsorption of malachite green (MG). The effects of concentration in equilibrium, and influent flow rate (15–30 mL/min), initial concentration (20–80 mg/L) and bed height (2–6 cm) in dynamics mode were investigated. SSAC with surface area of 979 m²/g shows an outstanding maximum capacity of malachite green at 530 mg/g. In adsorption dynamics, the breakthrough time and bed capacity increased with increasing bed height, and decreasing flow rate and influent dye concentration. Bohart-Adams, Thomas, Yoon-Nelson and Clark models were applied to describe the column breakthrough, dynamics behaviour and adsorption mechanisms. The breakthrough curves were best fitted by Yoon-Nelson model at the experimental conditions. The maximum bed capacity was reported to be 565 mg/g. SSAC is an effective adsorbent for MG removal from aqueous phase.

Keywords Activated carbon · Adsorption · Sawdust · Textile sludge · Malachite green · Wastewater treatment

1 Introduction

Malachite green (MG), a blueish green cationic dye, has been widely used to impart colour in paper and fabric industries. MG is soluble in water, toxic and recalcitrant to biological degradation. It deteriorates water quality and impedes sunlight penetration in streams. This consequently impairs the photosynthetic activities, hence decreasing the dissolved oxygen levels for respiration of aquatic living creatures. Eventually, the whole aquatic ecosystem and food chain will be compromised. Amongst other wastewater treatment strategies, MG can be effectively removed through adsorption using activated carbon [8, 26].

Adsorption is a simple and cost-competitive process in terms of design, operation and maintenance. However, the costly commercial activated carbon prompts tremendous

endeavours to develop cheaper substitutes, especially from biomass and industrial waste such as waste *Elaeagnus* stone [23], wood [52], cactus cladodes [15], waste printed circuit boards [29], coal fly ash and waste aluminium foil [12]. Sawdust and textile sludge are examples of freely and abundantly available promising materials for activated carbon preparation. In this work, textile sludge–sawdust chemically produced activated carbon (SSAC) in granular was evaluated for MG removal in batch and column adsorption systems.

Batch adsorption is crucial in understanding the interaction on activated carbon surface in relation to its surrounding dye concentration at equilibrium [38]. Column adsorption, on the other hand, is useful to shed further insight into industrial applications [25]. Unlike batch mode, the dynamics operation mainly relies upon bed saturation which is less likely to run under equilibrium [25, 57]. Precise modelling of dynamics pattern based on fundamental mass transport mechanism (surface, pore and film diffusion) is therefore indispensable in designing a continuous adsorption process.

This work was aimed to evaluate the equilibrium and dynamics of MG adsorption by SSAC. Isotherm models, namely Langmuir, Freundlich, Temkin and Redlich-Peterson, were used to interpret the equilibrium data and possible mechanisms governing the removal of MG. In dynamics mode, kinetic models, i.e. Bohart-Adams, Thomas, Yoon-Nelson and Clark models, were employed to describe the breakthrough

✉ Muhammad Abbas Ahmad Zaini
abbas@cheme.utm.my

Tang Shu Hui
shtang1991@gmail.com

¹ Centre of Lipids Engineering & Applied Research (CLEAR), Ibnu-Sina Institute for Scientific & Industrial Research (ISI-SIR), Universiti Teknologi Malaysia, 81310 Johor Bahru, Johor, Malaysia

² School of Chemical & Energy Engineering, Faculty of Engineering, Universiti Teknologi Malaysia, 81310 Johor Bahru, Johor, Malaysia

curves. The effects of initial concentration, influent flow rate and bed height on the bed capacity and dynamics behaviour were evaluated and discussed.

2 Material and methods

Textile sludge was obtained from textile factory, while sawdust was supplied by wood production factory, both located in Johor state of Malaysia. Hydrochloric acid (30%), phosphoric acid (85%), potassium hydroxide and malachite green were obtained from R&M Marketing, Essex, UK. Sodium hydroxide (96%) was purchased from Bendosen and potassium iodide was supplied by QRec (Asia). All chemicals are reagent grade, and were used without further purification.

2.1 Preparation of activated carbon granule (SSAC)

Based on previous works, the ratio of 0.7:0.3:1 (KI:KOH:TS) produced high surface area AC with the best MG adsorption capacity [48], while the ratio of 1.7:1 (H₃PO₄: sawdust) produced pellets with high surface area, MG adsorption and compression strength [49]. In this work, textile sludge (TS) was dried at 110 °C for 48 h, crushed and sieved to a size of 178 µm. It was mixed with chemical solution at mass ratio of 0.7:0.3:1 (KI:KOH:TS), followed by heating at 90 °C for 1.5 h. The impregnated sample was activated at 700 °C for 1 h. The activated carbon powder (labelled as AC) was soaked in HCl, and rinsed using distilled water until the solution pH is constant. After that, it was oven-dried at 110 °C.

Sawdust was mixed with 60 wt% H₃PO₄ solution at mass ratio of 1.7:1 (H₃PO₄:sawdust). Then, AC was added at mass ratio of 1:0.4 (sawdust:AC). The mixture was stirred at 85 °C for 1 h. A 3 g of solid from the mixture was separately pressed into a 10 mm inner diameter cylindrical mould. Then, the sample was heated at 560 °C for 3 h. The resultant pellets were washed with distilled water to remove excess H₃PO₄, and dried in a desiccator at room temperature for 26 h. Finally, it was reduced to a uniform granule size of 0.5 mm (labelled as SSAC).

2.2 Characterization of SSAC

The textural properties of activated carbons were determined by N₂ gas adsorption at 77 K in a pressure range of 10⁻⁵ to 0.995 using a MicroActive analyser. The carbon material was initially degassed at 300 °C for 24 h. The Brunauer-Emmett-Teller (BET) model was applied to calculate the surface area and mesopore volume of SSAC. The surface morphology was obtained by scanning electron microscope (model SEM-50, Philips, Holland). Boehm titration and pH_{pzc} were carried out to investigate the surface functional groups and net surface

charge of SSAC. In Boehm titration, 0.3 g of pellet was added into 15 mL of 0.1 M NaHCO₃, 0.05 M Na₂CO₃, 0.1 M NaOH and 0.1 M HCl solutions. The mixture was shaken for 48 h to achieve equilibrium. A 5 mL of the supernatant was pipetted, and back-titrated with 0.05 M HCl or 0.1 M NaOH, respectively. Phenolphthalein and methyl red were used as pH colour indicators. Back titration was performed for each reaction bases due to the difficult removal of CO₂ from solutions [24, 37]. The pH_{pzc} was elicited by pH drift method. The pellet was added into 50 mL of 0.1 M NaCl solution of varying pH (2 to 12), wherein the pH was adjusted using 0.1 M HCl and 0.1 M NaOH. The mixture was agitated for 24 h, and the final pH was measured and recorded. The point where the initial pH is equal to final pH is the value of pH_{pzc}.

2.3 Adsorption studies

A 0.05 g of SSAC was added into 50 mL of MG dye solution of varying concentrations. The solid-solution mixture was agitated in a shaker at 120 rpm and room temperature for 72 h. Subsequently, the final concentration was measured using a visible spectrophotometer (Spectrumlab 752Pro) at λ_{max} = 650 nm. The adsorption capacity, *q_e* (mg/g), was computed as,

$$q_e = \frac{C_o - C_e}{W} V \quad (1)$$

where *C_o* and *C_e* (mg/L) are the initial concentration and equilibrium concentration of dye solution, respectively, *V* (L) is the volume of dye solution and *W* (g) is the mass of SSAC.

A fixed quantity of SSAC was loaded into a fabricated acrylic column (56 cm height and 0.7 cm inner diameter) to get the required adsorbent bed height. Then, a stainless-steel wool was placed at the top and bottom of adsorbent bed to secure the close packed arrangement and prevent loss of adsorbent. Both column ends were closed with threaded caps, connecting them to a peristaltic pump to feed the influent MG solution at a desired upward flow rate through the vertical column. The MG feed solution was injected in an upward flow to avert channelling due to gravity. The setup of fixed-bed adsorption is shown in Fig. 1. A series of tests were performed to investigate the effects of operating parameters such as flow rate (*F* = 15, 20, 30 mL/min), bed height (*H* = 2, 4, 6 cm) and inlet concentration (*C_o* = 20, 50, 80 mg/L) on the dynamics behaviour and volumetric adsorption capacity of MG by SSAC adsorbent. The natural pH of MG solution was maintained in the range of 3 to 5. The samples were collected at regular intervals and the concentrations were measured accordingly. When the effluent concentration exceeded a value of 99.5% of its initial concentration, the column operation was halted.

The breakthrough (C_t/C_o) was plotted against time, t , where C_o (mg/L) is the influent concentration, C_t (mg/L) is the effluent concentration at service time, t . The breakthrough time, t_b is defined as the time at which the effluent concentration reached approximately 10% of the influent concentration ($C/C_i \approx 0.1$) [9, 21] to assess the breakthrough curves. The breakthrough and saturation points corresponding to the influent concentration were set at 10 and 95%, respectively. The total volume of treated effluent, V_{eff} (mL) was determined as,

$$V_{eff} = Q t_{total} \tag{2}$$

where Q and t_{total} represent the volumetric flow rate (mL/min) and the total flow time (min), respectively. The total amount of MG adsorbed, q_{total} (mg) was obtained by reckoning the area, A under the curve of concentration of adsorbed MG, C_{ad} (mg/L) at time t , which is $C_{ad} = C_o - C_t$ versus time t (min). The mathematical expression is shown below [47].

$$q_{total} = \frac{QA}{1000} = \frac{Q}{1000} \int_{t=0}^{t=t_{total}} C_{ad} dt \tag{3}$$

The equilibrium MG uptake or adsorption capacity, q_e (mg/g) was computed as,

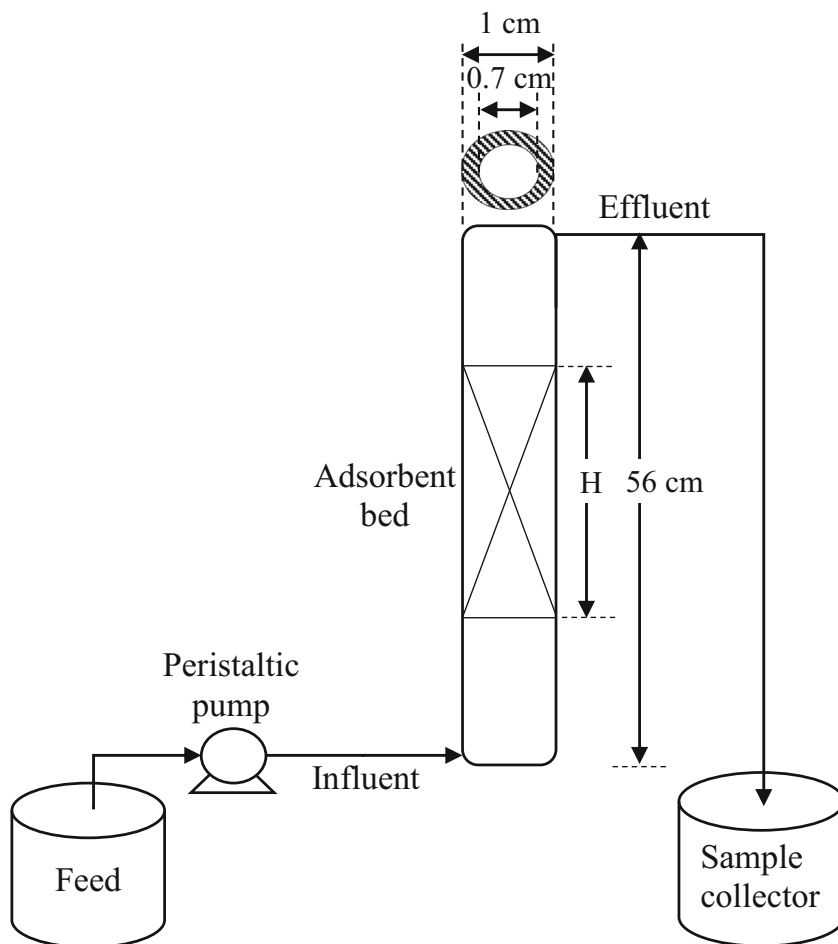
$$q_e = \frac{q_{total}}{m} \tag{4}$$

where m (g) is the mass of SSAC in the column. The mass transfer zone (MTZ) is section inside the column where the MG concentration decreased from 90 to 10% of the inlet concentration. It is where most of the mass transfer or adsorption happens and it moves from zero (front or inlet) to saturation (back end) [35]. The length of MTZ or the unused bed length, H_{UN} (cm) was computed as,

$$H_{UN} = H \left(1 - \frac{t_b}{t_s} \right) \tag{5}$$

where H (cm) is the total bed height, t_b (min) is the time at breakthrough and t_s (min) is the saturation time. The total amount of MG fed to the column, W_{total} (mg) was calculated from the equation,

Fig. 1 The fixed-bed adsorption setup



$$W_{\text{total}} = \frac{C_o Q_{t_{\text{total}}}}{1000} \quad (6)$$

The total MG removal, R (%) was computed from the ratio of the total amount MG adsorbed, q_{total} to the total amount of MG fed to the column, W_{total} as expressed below.

$$R (\%) = \frac{q_{\text{total}}}{W_{\text{total}}} \times 100 \quad (7)$$

In this work, three mathematical models—Bohart-Adams, Thomas, Yoon-Nelson and Clark models—were used to predict the column breakthrough curves of adsorbent and explain the mechanisms of continuous adsorption. Microsoft Excel solver was utilized for data processing for non-linear regression analysis. The mathematical expressions and the assumptions are summarized in Table 1.

3 Results and discussion

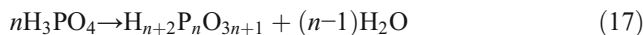
3.1 Reaction mechanism of SSAC

Textile sludge was activated with KOH at 700 °C following the reaction mechanism below [53],



Thus, H_2 , CO_2 and CO are released, and porous activated carbon is formed.

The activated carbon powder is then converted into granules by mixing with H_3PO_4 and sawdust. According to Li et al. [30], dehydration of H_3PO_4 occurs at temperature of 100 to 400 °C.



At temperature of 400 to 700 °C, $\text{H}_{n+2}\text{P}_n\text{O}_{3n+1}$ dehydrates into P_4O_{10} and it reacts with carbon, creating new pores, enlarging the existing pores and releasing CO_2 [30].



3.2 Characteristics of SSAC

Table 2 shows the yield, textural properties and pH of SSAC prepared at 560 °C and 3 h. The mass of the sample decreased after carbonisation with 59% yield due to the gasification of carbon into CO and CO_2 , devolatilization and carbon-chemical reaction. These reactions caused multiple pores to develop and consequently increase the surface area and other textural properties of the SSAC as shown in Table 2. The high S_{BET} , V_T and PD_{avg} of SSAC facilitates greatly in the removal capacity of MG dye molecules. MG has a molecular diameter of 1.26 nm [51], hence the average pore diameter of the adsorbent should be at least 2 times [34] of the MG molecules (2.5 nm) for smooth pore diffusion. SSAC has a PD_{avg} of 2.77 nm, making it advantageous for the adsorption of MG. Figure 2 displays the pore size distribution graph of SSAC with two peaks at 2 nm and 3.8 nm, denoting that it is predominantly mesoporous (pore width in the range of 2 nm to 5 nm).

Table 1 Column adsorption models [11, 17, 50, 54, 56, 58]

Dynamics model	Assumption	Equation
Clark model	The shape of the mass-transfer zone is constant and all the adsorbates are removed at the end of the column.	$\frac{C_t}{C_o} = \left(\frac{1}{Ae^{-kt} + 1} \right)^{\frac{1}{n-1}}$ (8)
Thomas model	Freundlich isotherm defines the sorption behaviour of adsorbate. The sorption rate is determined by the outer mass transfer step. Assumes the second-order reversible reaction kinetics and the Langmuir isotherm.	$\frac{C_t}{C_o} = \frac{1}{e^{k_T} \frac{q_o m}{Q k_T} C_o t + 1}$ (9)
Bohart-Adams model	Plug flow manner in adsorbent bed. The uptake rate of adsorbate is proportional to the concentration of the adsorbate existing in the bulk fluid and the residual adsorptive capacity of adsorbent.	$\frac{C_t}{C_o} = e^{k_{BA} \frac{C_o t}{e^{k_{BA}} N_o} \frac{Z}{U} - 1} + e^{k_{BA}} C_o t$ (10)
Yoon-Nelson model	The reaction is not immediate as the model is based on the theory of surface reaction. The rate of decrease in the probability of adsorption for each adsorbate molecule is proportional to the probability of its adsorption and breakthrough on the adsorbent. Applicable for single component system.	$\frac{C_t}{C_o} = \frac{1}{e^{k_{YN}(t-\tau)} + 1}$ (11)

Table 2 Yield, textural properties and pH of SSAC

Yield (%)	58.6
S_{BET} (m ² /g)	979
Mic. (%)	15.8
V_T (cm ³ /g)	0.678
D_{avg} (nm)	2.77
pH	3.2
q_m (mg/g)	530

S_{BET} BET surface area, V_T pore volume, D_{avg} average pore diameter

Figure 3 shows the scanning electron microscopy (SEM) images of SSAC. Irregular cavities and minimal crevices can be seen on the external morphology of SSAC surface which is caused by the evaporation of phosphoric acid and decomposition of organic matters during carbonisation. The white particles can be attributed to the leftover phosphate or other metal compounds on activated carbon [5]. H₃PO₄-modified coconut shell AC [5] and H₃PO₄-activated rice husk char [2] exhibited similar morphology with SSAC. The addition of AC minimizes the aggregation of the glutinous tar [49] which may block the pores, resulting in better adsorption of MG.

The surface functionality analysis via Boehm titration showed that SSAC contains 1.6 mmol/g of acidic groups and 0.123 mmol/g of basic groups. The greater amount of acidic functional groups reduces the pH_{pzc} and pH of the SSAC, revealing a negatively charged surface in solution. On the other hand, the presence of the basic groups resulted from the indirect alteration of the surface functionality by H₂O and CO₂ released during carbonisation.

Figure 4 illustrates the deduction of pH_{pzc} of the SSAC using pH drift method. It can be seen that the pH_{initial}/pH_{final} plots levelled off at pH range of 4 to 10 and the pH_{pzc} was approximately 2.1, whereas the pH is 3.2. The low pH_{pzc} of SSAC is attributed to its higher amount of acidic functional groups and only some basic groups were present. The acidic and basic surface functional groups of the SSAC are influenced by the activation technique and the type of precursor

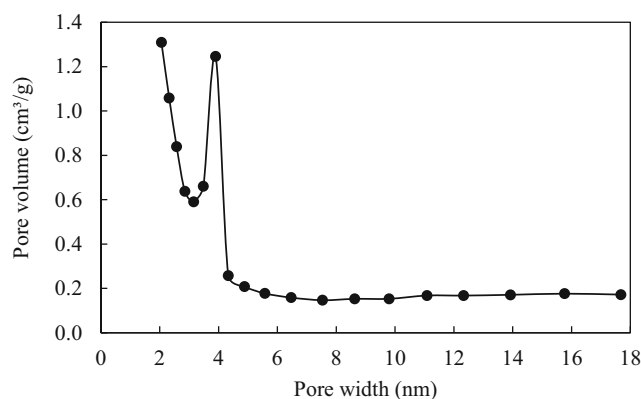


Fig. 2 Pore size distribution of SSAC

(sawdust and TS) used. In this study, the solution pH is greater than the pH_{pzc}, signifying that the negatively charged surface of SSAC creates greater affinity towards MG cations. The SSAC is a L-type AC as their pH is greater than pH_{pzc}. In other words, it is hydrophilic and generates negative charges in aqueous solution [14].

3.3 Equilibrium isotherm

Figure 5 shows that the experimental data and the Langmuir plot of the SSAC performed at initial concentration of 50–900 mg/L and 25 °C for 72 h. It can be seen that the equilibrium adsorption capacity, q_e with increasing concentration with a decreasing gradient until an equilibrium was attained, signifying the saturation point. The q_e is small at low concentrations as the amount of MG molecules available for adsorption sites is the limiting factor. At high concentrations, the active sites for adsorption quickly become saturated until the equilibrium is achieved and no further adsorption occurs. The excellent MG adsorption capacity of SSAC was ascribed to its higher surface area, large average pore diameter (with respect to MG molecules) and the negatively charged surface. These physicochemical properties of SSAC maximize the utilization of the adsorption sites, making the adsorption intense and rapid. The high of MG towards SSAC was also evident through the 90° Langmuir plot, whereby the plot is close to the ordinate.

Langmuir, Freundlich, Redlich-Peterson and Temkin isotherms were selected for the fitting of the equilibrium data. The respective equations are given as follows.

$$q_e = \frac{q_m b C_e}{1 + b C_e} \tag{20}$$

$$q_e = K_F C_e^{1/n} \tag{21}$$

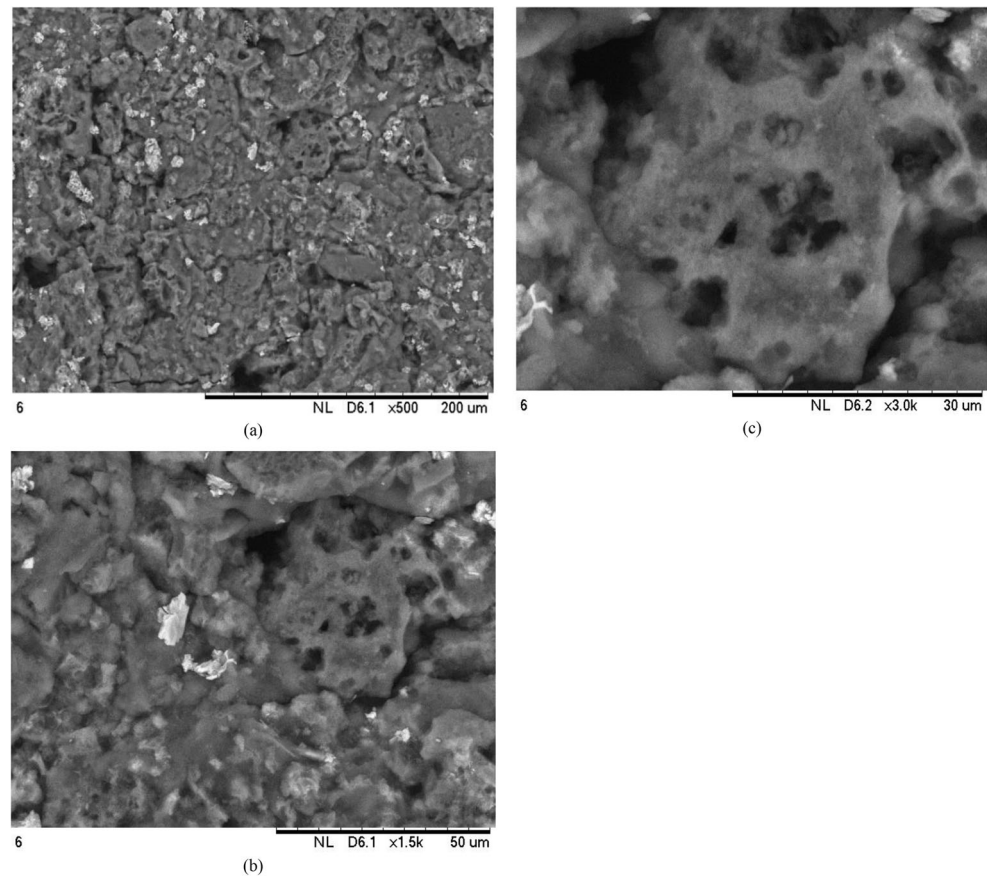
$$q_e = \frac{K_R C_e}{1 + a_R C_e^g} \tag{22}$$

$$q_e = \frac{RT}{b_T} \ln(A_T C_e) \tag{23}$$

The fitting results are summarized in Table 3. The Langmuir isotherm equation provided an excellent fit with high R^2 value of 0.915 and low root mean square error (RMSE) compared to other isotherms, indicating the adsorption of MG onto the SSAC is monolayer. Langmuir constant b is related to the affinity between MG and SSAC. As shown in Fig. 5, the adsorption curve is closer to the q_e axis of the graph at lower concentrations, implying that the adsorption process is more favourable or spontaneous due to greater affinity at these conditions.

The Freundlich isotherm is the least appropriate model, implying that the multilayer formation of MG onto a

Fig. 3 SEM images of SSAC at different magnifications



heterogeneous surface is improbable. n and K_F are associated with the sorption intensity and sorption capacity of the adsorbent [27]. The n value for SSAC is 5.14, with the $1/n$ value below one, indicating a standard Langmuir isotherm [40]. This finding confirmed that the Langmuir isotherm is a good fit.

The Temkin isotherm yielded satisfactory R^2 and RMSE values. Among the Temkin constants, R is the universal gas

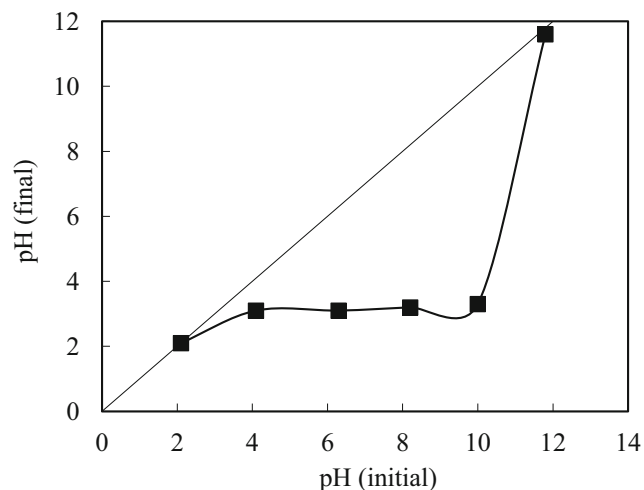


Fig. 4 pH_{pzc} of SSAC by pH drift method

constant (8.314 J/mol K), A_T is equilibrium binding constant related to the maximum binding energy and B is related to the heat of sorption, in which $B = RT/b_T$. The B , b_T and A_T values were tabulated in Table 3. The B value is less than 97 J/mol, suggesting that the adsorption of MG onto SSAC is a physisorption [41].

Redlich-Peterson (R-P) is a three-parameter empirical equation which merges the Langmuir and Freundlich models [42]. g , a_R and K_R are the Redlich-Peterson constants and their values can be found in Table 3. The g value of SSAC 1. When

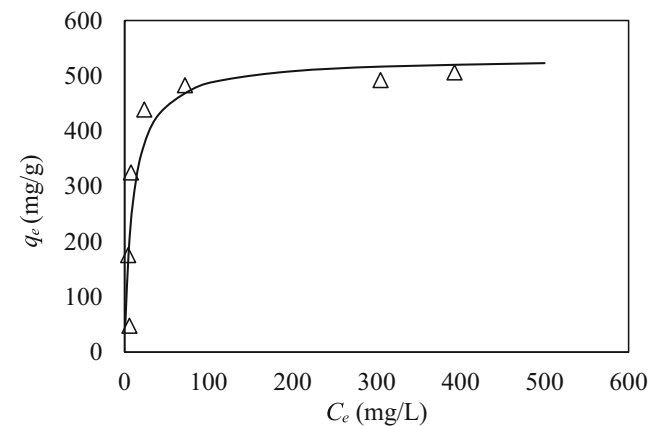


Fig. 5 Equilibrium adsorption of MG by SSAC (data were fitted using Langmuir model)

Table 3 Isotherm parameters for MG adsorption onto SSAC

	Langmuir	Freundlich		Temkin		Redlich-Peterson		
q_m (mg/g)	530	n		5.14	B (J/mol)	80.1	K_R (L/g)	65.8
b (L/mg)	0.124	K_F (mg/g) (L/mg) ^{1/n}	173	b_T	31.5	a_R (L/mg) ^g	0.124	
R^2	0.915	R^2	0.687	A_T (L/g)	2.71	g	1.00	
RMSE	54.3	RMSE	100	R^2	0.778	R^2	0.915	
				RMSE	84	RMSE	54.3	

$g = 1$, the R-P equation is simplified to the Langmuir equation, whereby K_R (R-P) represents $q_m b$ (Langmuir), and a_R (R-P) is similar to b (Langmuir) [6, 55]. The Langmuir constants were consistent with the R-P constants as exhibited in Table 3. According to Wu and co-workers, the value of g is nearly unity in the adsorption of large molecules especially dyes owing to the solid hindrance between pores and adsorbate molecules [55]. Both Langmuir and R-P models provided excellent fitting with the best R^2 values and lowest RMSE, thus confirming the single layer MG formation on SSAC as the predominant adsorption equilibrium mechanism.

3.4 Adsorption dynamics

Continuous fixed-bed column study was carried out to give further practical and operational information for the industrial scaling up purposes. The effects of design process parameters including bed height, influent flow rate and dye concentration on the breakthrough curves (BTCs) were studied using SSAC. The experimental data were fitted into Thomas, Yoon-Nelson, Bohart-Adams and Clark kinetics models, and the dynamics parameters were determined under various process conditions.

The effect of influent of MG concentration (20, 50, 80 mg/L) on the BTCs was studied at fixed flow rate of 20 mL/min and bed height of 2 cm. As can be seen from

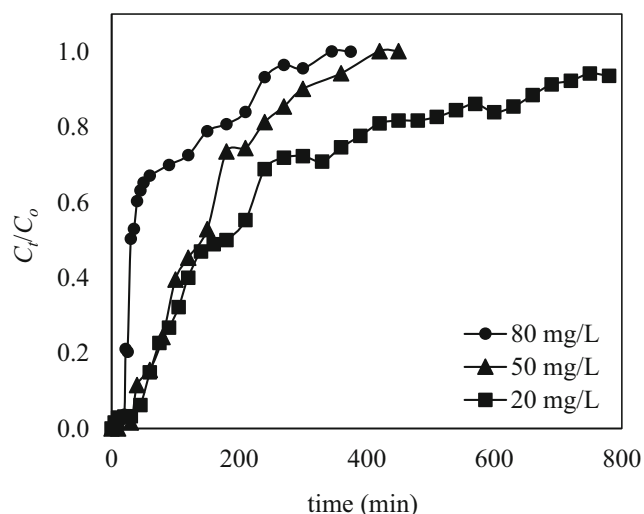


Fig. 6 BTCs at different influent MG concentrations (flow rate = 20 mL/min, bed height = 2 cm (0.318 g), temperature = 25 °C)

Fig. 6, the shape of the BTC becomes steeper as influent concentration increased from 20 to 80 mg/L signifying that the MTZ is small and the adsorption is mainly governed by the slow intraparticle diffusion [1, 13, 21]. A higher concentration gradient supplies a greater driving force in assisting the migration process to overpower the mass transfer resistance, thus facilitating the film diffusion.

Table 4 shows the BTC parameters for MG adsorption onto SSAC at different conditions. Higher influent concentrations reduce the breakthrough and saturation time, treated volume of effluent and the percentage of MG removal, while the equilibrium uptake augments. Since the bed height or mass of adsorbent is fixed, the limited active binding sites can only adsorb a fixed amount of MG. Consequently, the adsorbent bed becomes saturated rapidly at higher concentration, where more MG molecules are left unadsorbed, causing an earlier breakthrough and saturation of adsorbent bed, and less purified effluent. The increase in adsorption uptake of MG is attributed to the higher concentration gradient which boosts the MG transport or diffusion rate [3, 7]. Similar trends were also elicited from the removal of methylene blue dye using *Eucalyptus sheathiana* bark biomass [1], adsorption of tricaine methanesulfonate onto pyrolysed paper mill sludge [21] and Cd (II) and Cu (II) ions adsorption onto palm oil boiler mill fly ash [7].

The BTCs at different influent flow rates (15, 20 and 30 mg/L) and constant concentration (50 mg/L) and bed height (2 cm or 0.318 g) are depicted in Fig. 7, while the BTC parameters can be found in Table 4. As the flow rate augments, the BTC becomes steeper with shorter breakthrough and saturation time. At a high flow rate, the residence time of MG dye molecules in the column is insufficient to achieve equilibrium, wherein the front adsorption region or MTZ moves swiftly to the end (or top) of the column, causing the adsorbent bed to saturate faster [1, 21]. As a result, the MG dye solution exits the column before the equilibrium happens, which is characterized by the larger MTZ. This leads to the lower equilibrium adsorption capacity and MG removal efficiency as shown in Table 4. On the other hand, a lower influent flow rate allows enough contact time between MG dye molecules and the adsorbent bed, leading to a smaller MTZ and higher equilibrium uptake and removal percentage of MG.

Table 4 BTC parameters for the removal of MG using SSAC granules (0.5 mm) in fixed-bed column at different inlet concentrations, flow rates and bed heights

C_o (mg/L)	Q (mL/min)	H (cm)	V_{eff} (mL)	t_b (min)	t_s (min)	H_{LN} (cm)	q_{total} (mg)	q_e (mg/g)	R (%)
20	20	2	16,800	53	750	1.86	114	360	34
50			9000	34	469	1.86	150	472	33
80			7500	21	335	1.87	160	503	27
50	15	2	8100	44	497	1.82	171	538	42
	20		9000	34	469	1.86	150	472	33
	30		10,800	16	312	1.90	133	419	25
50	20	2	9000	34	469	1.86	150	472	33
		4	12,600	142	541	2.95	317	504	50
		6	19,600	327	918	3.86	539	565	55

The bed height affects the dynamics behaviour and quantity of MG captured. The column adsorption experiments were carried out at bed heights of 2, 4 and 6 cm (0.318, 0.636 and 0.954 g). The influent flow rate and concentration were fixed at 20 mL/min and 50 mg/L. Figure 8 shows that as the bed height increases, the BTC becomes slightly less steep with significantly longer breakthrough and saturation time, resulting in the larger volume of treated effluent, and increased MG uptake and percentage removal (Table 4). This is because a higher bed height prolongs the residence time of MG solution inside the column, broadens the MTZ and lengthens the distance of MTZ, shifting from the front to the end of the bed [3, 4]. Therefore, more MG dye molecules could diffuse deeper into the internal pores of SSAC; consequently, a higher MG removal efficiency is attained. Moreover, a higher bed height or larger mass of SSAC also increases the contact surface area, which enhances the availability of additional binding sites for the adsorption of MG molecules. Nevertheless, axial dispersion controls the mass transfer at lower bed height, causing not enough time for MG molecules to diffuse into the adsorbent bed [1, 7]. As a result, the breakthrough occurred

within a short time. This can also be justified through the increase of MTZ region at higher bed heights as shown in Table 4.

Modelling of column adsorption was performed to forecast the dynamics operation of the fixed-bed column and predict the kinetics coefficients. The model parameters were calculated by non-linear regression analysis, and the values are tabulated in Table 5.

The Thomas model gave a good fitting with coefficient of determination (R^2) of up to 0.983 and low root mean square error (RMSE), indicating insignificant radial and axial dispersion, constant void fraction, negligible temperature and pressure change inside the fixed-bed column [22]. Besides, it is also suggested that the intraparticle and external diffusion are not the rate-limiting steps due to extremely small resistance [1, 10, 22]. The adsorption capacity of the bed (q_o) increased and the Thomas rate constant k_T decreased with decreasing flow rate. This is because lower flow rate enables longer residence time inside the column, allowing the MG dye molecules sufficient time to diffuse into the pores of SSAC, therefore

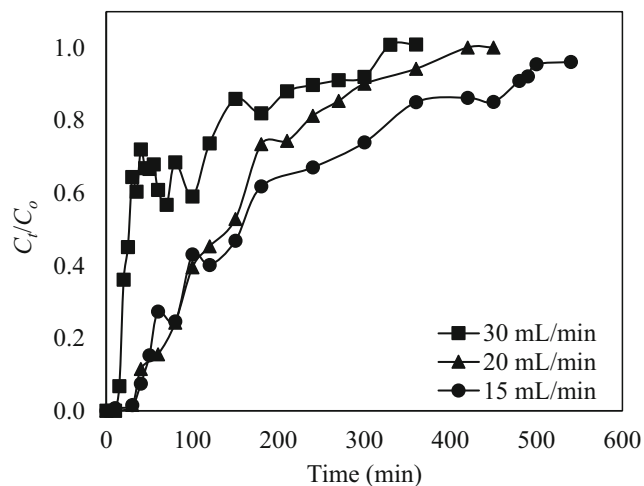
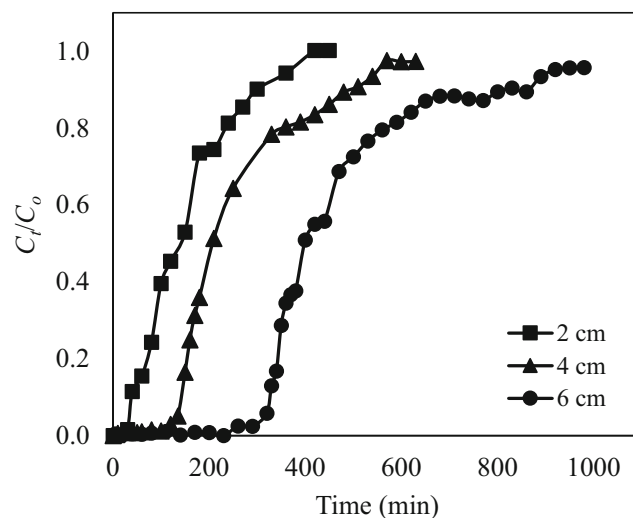
**Fig. 7** BTCs at different influent flow rates (influent concentration = 50 mg/L, bed height = 2 cm (0.318 g), temperature = 25 °C)**Fig. 8** BTCs at different bed heights (flow rate = 20 mL/min, influent concentration = 50 mg/L, temperature = 25 °C)

Table 5 Thomas, Yoon Nelson, Bohart-Adams and Clark model parameters at various flow rates, influent concentrations and bed heights

Model	Parameter	C_o (mg/L)			Q (L/min)			H (cm)		
		20	50	80	15	20	30	2	4	6
Thomas	q_{exp} (mg/g)	360	472	503	538	472	419	472	504	565
	q_o (mg/g)	299	437	220	483	437	224	437	424	520
	k_T (mL/min.mg)	0.386	0.383	0.821	0.197	0.383	0.415	0.383	0.267	0.222
	R^2	0.941	0.983	0.908	0.952	0.983	0.732	0.983	0.974	0.979
	RMSE	0.090	0.053	0.146	0.083	0.053	0.152	0.053	0.073	0.068
Yoon Nelson	$t_{50\%}$ (min)	180	139	32.7	156	139	22.7	139	198	388
	τ (min)	214	142	41.5	177	142	43.2	142	242	432
	k_{YN} (1/min)	0.009	0.019	0.069	0.011	0.019	0.023	0.019	0.015	0.013
	R^2	0.941	0.983	0.908	0.952	0.983	0.732	0.983	0.974	0.979
	RMSE	0.090	0.053	0.146	0.083	0.053	0.152	0.053	0.073	0.068
Bohart Adams	$N_o \times 10^{-4}$ (mg/L)	15.4	34.8	56.5	49.6	34.8	30.1	34.8	35.0	37.4
	$k_{BA} \times 10^5$ (L/mg min)	18.40	7.15	5.02	4.97	7.15	8.34	7.15	6.68	4.46
	R^2	0.911	0.921	0.695	0.909	0.921	0.643	0.921	0.906	0.879
	RMSE	0.153	0.264	0.270	0.248	0.264	0.212	0.264	0.268	0.264
Clark	A	1126	8908	25,501	2083	8908	77	8908	6.41×10^6	1.34×10^7
	r (1/min)	0.019	0.042	0.172	0.026	0.042	0.035	0.042	0.058	0.031
	R^2	0.907	0.958	0.885	0.924	0.958	0.678	0.958	0.972	0.968
	RMSE	0.118	0.084	0.160	0.110	0.084	0.166	0.084	0.099	0.090

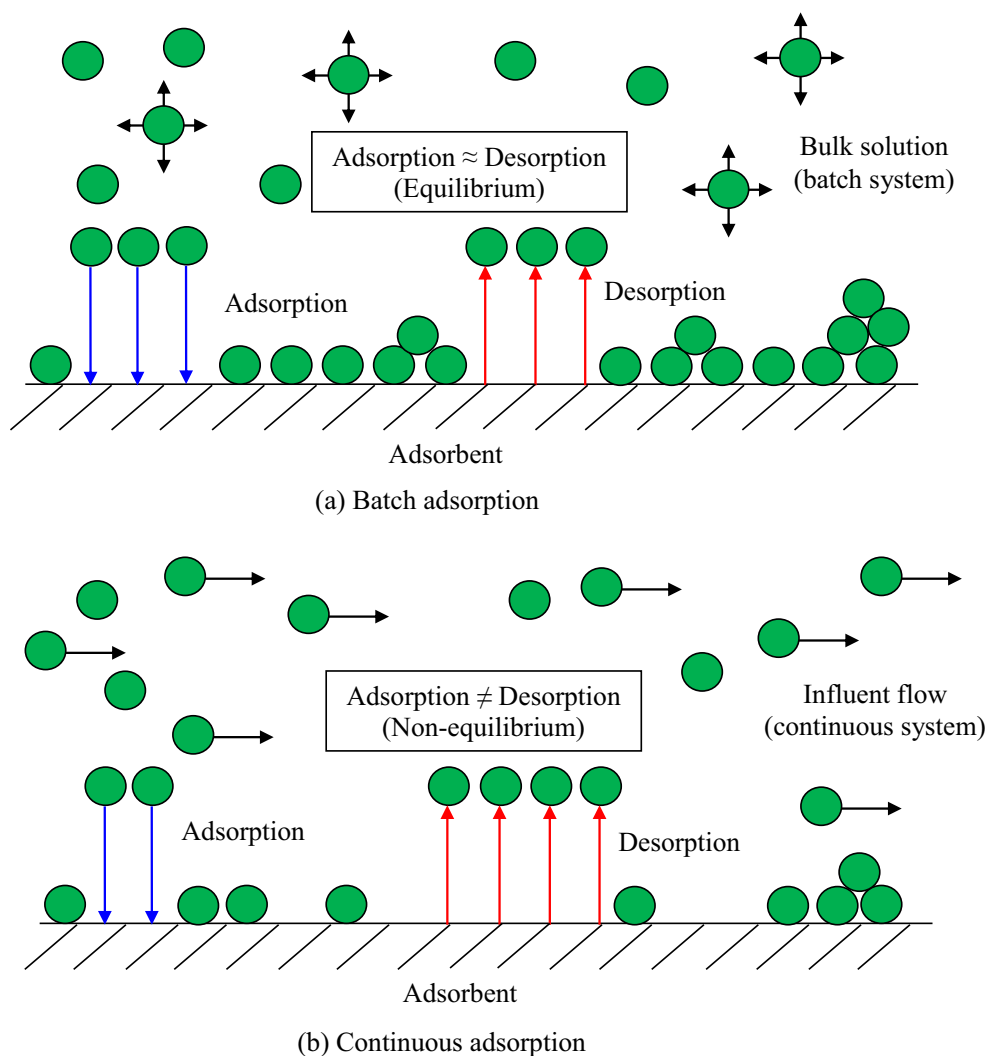
boosting the adsorption capacity. The q_o also increased, while k_T decreased as the influent concentration and bed height increased. The higher influent concentration enhances the driving force, and the higher bed height provides more adsorption sites, resulting in the greater bed capacity. The lower q_o is attributed to the surging competition between the MG dye molecules as the adsorption sites on SSAC were slowly occupied. The experimental q_e and calculated q_o did not differ significantly except at high flow rate (30 mL/min) and high influent concentration (80 mg/L) as the external diffusion resistance may not be negligible at these conditions, therefore breaking the assumption in the Thomas model. The values of k_T (0.197–0.821 mL/min.mg) and q_o (220–550 mg/g) in this work were comparable with other studies. Ferreira and co-workers (2017) reported the k_T values of 0.167–0.4 mL/min mg and q_o values between 85.6 and 108 mg/g for tricaine methanesulfonate adsorption using pyrolysed paper mill sludge at different column conditions (bed depth = 4.5, 9.0, 13.0 cm; influent concentration = 100, 250, 400 mg L⁻¹; flow rate = 15, 27, 56 L/min). Furthermore, Jerold et al. [28] also discovered k_T values between 0.069 and 0.163 mL/min mg and q_o values of 328–565 mg/g for adsorption of malachite green onto nano zerovalent iron algal biocomposite at various bed height (3–9 cm), flow rate (5–15 mL/min) and initial MG concentration (5–15 mg/L).

The Yoon-Nelson model also provides a good fit and the R^2 and RMSE values were coincidentally similar to that of the Thomas model. Ferreira et al. [21] and Aziz et al. [7] also

reported the same observation for tricaine methanesulfonate removal onto pyrolysed paper mill sludge, and column adsorption of Cd(II) and Cu(II) ions onto palm oil boiler mill fly ash, respectively. From Table 5, Yoon-Nelson rate constant (k_{YN}) increased with increasing influent flow rate and dye concentration, but decreased with increasing bed height. The rise in k_{YN} values can be attributed to the greater force controlling the mass transfer in the liquid phase at high influent concentration and flow rate [31]. Meanwhile, the 50% breakthrough time required (τ) decreased with increasing flow rate and influent concentration, but it increased with increasing bed height. This is because at high influent flow rate and concentration, more MG dye molecules are channelled to the adsorbent bed with limited adsorption sites, causing rapid exhaustion of the adsorbent and earlier 50% breakthrough (τ), while higher adsorbent bed height provides abundant adsorption sites available for adsorption of the MG molecules, therefore extending the τ . Such pattern in both k_{YN} and τ were also widely noticed in other research [1, 7, 21, 22, 45]. The computed and experimental values of τ or $t_{50\%}$ were in close approximation. The high R^2 and low RMSE values implied that the column adsorption behaviour of MG onto SSAC was well illustrated by the Thomas and Yoon Nelson models.

The Bohart-Adams model is generally the least suitable column adsorption model to describe the BTC owing to its lowest R^2 and highest RMSE values. It is evident from Table 5 that the saturation concentration (N_o) decreased with increasing flow rate, but increased with increasing influent

Fig. 9 Adsorption mechanism in **a** batch and **b** continuous operations



concentration and bed height because insufficient residence time at high flow rate deteriorates the adsorption efficiency, while greater driving force caused by concentration gradient at high influent concentration and plentiful free adsorption sites at higher bed height improve the N_o . On the other hand, the

Bohart–Adams kinetic constant (k_{BA}) decreased with increasing influent concentration and bed height, but increased with increasing flow rate signifying external mass transfer governs the overall system kinetics in the initial phase of the adsorption in the column [10, 22]. The increase of k_{BA} at higher flow

Table 6 Surface area, bed capacity and breakthrough time of various adsorbents for continuous adsorption of cationic dyes

Adsorbent	Dye	S_{BET} (m ² /g)	C_o (mg/L)	q_{exp}	q_{Thomas} (mg/g)	t_b (min)	Best fit model	Ref
<i>Prosopis juliflora</i> seed AC	RB	1028	25–75	90.3	87.2	–	Yoon Nelson	[25]
Pine cone powder	MB	–	50–100	–	55.4	115	BDST	[57]
Rubber leaf powder	MB	–	–	96	99.2	167	Thomas	[16]
Pineapple leaf powder	MG	–	50–200	–	82.5	600	Thomas	[19]
<i>Avena sativa</i> (oat) hull	MG	63	25–200	69.3	69.3	1170	Thomas	[9]
<i>Eucalyptus sheathiana</i> bark biomass	MB	6.55	50–100	45.3	49.6	50	Thomas, Yoon Nelson	[1]
Granular AC	MG	1150	50–200	–	67.9	–	BDST model	[32]
Nano zerovalent iron algal biocomposite	MG	–	5–15	0.56	0.57	8.5	Thomas, Yoon-Nelson	[28]
SSAC	MG	979	20–80	565	520	327	Thomas, Yoon-Nelson	This study

AC activated carbon, RB rhodamine-B, MB methylene blue, MG malachite green, t_b breakthrough time

rate is attributed to the stronger kinetic energy of the MG dye molecules, while the closely packed MG molecules at higher influent concentration and the greater amount of adsorbent at higher bed height acts as a barrier to slow down the MG molecules, leading to weaker kinetic energy and decreasing k_{BA} . Similar trends of k_{BA} and N_o with correlation to flow rate, influent concentration and bed height were reported in several studies [22, 31, 39, 44]. In order to ensure better adsorption capacity per unit volume, N_o and smaller kinetic constant, k_{BA} (minimal resistance inside column) the flow rate ought to be lower with higher influent concentration and adsorbent bed height.

The Clark assumes that the adsorption dynamics follows the Freundlich isotherm and the outer mass transfer dominates the sorption rate [33]. The Freundlich constant (n) from the batch adsorption ($n = 5.04$) was used to calculate the parameters of the Clark model. The R^2 and RMSE values of the Clark model were found to be in the range of 0.68–0.97 and 0.08–0.17, respectively, reflecting that the Clark model provides a better fitting than the Bohart-Adams model, but is less appropriate than that of the Thomas and Yoon Nelson model. Table 5 shows that A decreased with increasing flow rate and decreasing influent concentration and bed height most likely due to the decline in adsorption efficiency at these conditions as rapid flow rate minimize the residence time, while low influent concentration limits the amount of MG dye and shorter bed height lowers the number of free active sites available for adsorption. On other hand, r increased with increasing flow rate and influent concentration as the higher flow rate reduces the external diffusion resistance and higher concentration induces greater driving force (due to concentration gradient), thus enhancing the rate of mass transfer. The same pattern was also reported in other studies [18, 36, 46].

3.5 Adsorption mechanisms

In this work, the maximum adsorption capacity of SSAC in the batch system is 530 mg/g and it is comparable with that of the continuous fixed-bed system at 360–565 mg/g. The adsorption performance difference between the batch and the fixed-bed systems is ascribed to the equilibrium establishment. In batch adsorption, the SSAC is in contact with a fixed amount of MG dye molecules for a time period until equilibrium is attained. In continuous fixed-bed adsorption, the MG solution flows into the column and exits before equilibrium is achieved at any phase (Fig. 9). The service time or the time where the MG molecules breakthrough reflects the adsorption efficiency in continuous fixed-bed operations [39]. Several studies also reported the varying adsorption capacities in both batch and fixed-bed operations [16, 20, 43].

3.6 Comparison with various cationic dyes adsorbents

Fixed-bed adsorption is the most common continuous column process utilized in various industrial applications for wastewater treatment purposes. Table 6 exhibited the surface area, breakthrough time and bed capacity of different adsorbents in the adsorption of cationic dyes at room temperature (30 °C) and natural solution pH. The highest bed capacity of SSAC in the fixed-bed adsorption of MG is 565 mg/g ($C_o = 50$ mg/L, $Q = 20$ mL/min, $H = 6$ cm) and is highly superior than other adsorbents like nano zerovalent iron algal bio-composite (0.56 mg/g) [28], *Avena sativa* (oat) hull (69.3 mg/g) [9] and pineapple leaf powder (85 mg/g) [19] as shown in Table 6. This signifies the powerful adsorptivity of SSAC in the continuous fixed-bed adsorption operation, which can be an excellent substitute for the commercial coal-based AC.

In short, it was found that high initial adsorbate concentration in influent, low flow rate and high bed height or depth were more favourable to ensure maximum bed adsorption capacity. Besides the operating parameters, the inherent physicochemical properties of the adsorbent also influence the performance of the adsorption column. It is proposed that the adsorbent should have large surface area and average pore diameter of more than 2 times that of the adsorbate to ensure easy and unrestricted mass transfer. Because of the dynamics behaviour and the insufficient time to achieve equilibrium in continuous mode, the adsorbent bed with opposite surface charge of the adsorbate is more desirable as the electrostatic attraction may improve the diffusion rate of adsorbate into the internal pores of the adsorbent.

4 Conclusion

The textile sludge–sawdust chemically produced activated carbon (SSAC) was produced for malachite green (MG) adsorption. The activated carbon has a surface area of 979 m²/g and yields a capacity of 530 mg/g at equilibrium. The column experiments showed that the bed capacity increased from 360 to 565 mg/g with decreasing flow rate (15–30 mL/min) and increasing influent concentration (20–80 mg/L) and bed height (2–6 cm). The highest bed capacity of 565 mg/g was achieved at initial concentration, flow rate and bed height of 50 mg/L, 20 mL/min and 6 cm (0.954 g), respectively. The dynamics behaviour was best illustrated by Yoon-Nelson models. In conclusion, SSAC is an excellent adsorbent for the treatment of MG in batch (equilibrium) and dynamics mode. The findings in this work are expected to contribute further understanding on dye wastewater treatment and waste utilization especially textile sludge and sawdust.

Acknowledgements This work was supported by UTM Shine Signaturare Grant No. 07G80. Tang Shu Hui is grateful for the UTM-Zamalah Scholarship for her PhD degree.

References

- Afroze S, Sen TK, Ang HM (2016) Adsorption performance of continuous fixed-bed column for the removal of methylene blue (MB) dye using Eucalyptusheathiana bark biomass. *Res Chem Intermed* 42(3):2343–2364
- Ahiduzzaman M, Islam AKS (2016) Evaluation of characteristics of activated carbon from rice husk impregnated with zinc chloride and phosphoric acid. *Am J Phys Chem* 5(5):94–98
- Ahmad AA, Hameed BH (2010) Fixed-bed adsorption of reactive azo dye onto granular activated carbon prepared from waste. *J Hazard Mater* 175(1–3):298–303
- Albroomi HI, Elsayed MA, Baraka A, Abdelmaged MA (2017) Batch and fixed-bed adsorption of tartrazine azo-dye onto activated carbon prepared from apricot stones. *Appl Water Sci* 7(4):2063–2074
- Anisuzzaman SM, Joseph CG, Taufiq-Yap YH, Krishnaiah D, Tay VV (2015) Modification of commercial activated carbon for the removal of 2, 4-dichlorophenol from simulated wastewater. *J King Saud Univ Sci* 27(4):318–330
- Ayawei N, Ebelegi AN, Wankasi D (2017) Modelling and interpretation of adsorption isotherms. *J Chem*. <https://doi.org/10.1155/2017/3039817>
- Aziz ASA, Manaf LA, Man HC, Kumar NS (2014) Column dynamic studies and breakthrough curve analysis for Cd (II) and Cu (II) ions adsorption onto palm oil boiler mill fly ash (POFA). *Environ Sci Pollut Res* 21(13):7996–8005
- Baek MH, Ijagbemi CO, Se-Jin O, Kim DS (2010) Removal of malachite green from aqueous solution using degreased coffee bean. *J Hazard Mater* 176(1):820–828
- Banerjee S, Sharma YC (2013) Equilibrium and kinetic studies for removal of malachite green from aqueous solution by a low cost activated carbon. *J Ind Eng Chem* 19(4):1099–1105
- Baral SS, Das N, Ramulu TS, Sahoo SK, Das SN, Chaudhury GR (2009) Removal of Cr (VI) by thermally activated weed *Salvinia cucullata* in a fixed-bed column. *J Hazard Mater* 161(2–3):1427–1435
- Bohart GS, Adams EQ (1920) Some aspects of the behavior of charcoal with respect to chlorine. 1. *J Am Chem Soc* 42(3):523–544
- Chatterjee A, Shamim S, Jana AK, Basu JK (2020) Insights into the competitive adsorption of pollutants on a mesoporous alumina-silica nano-sorbent synthesized from coal fly ash and a waste aluminium foil. *RSC Adv* 10(26):15514–15522
- Chen N, Zhang Z, Feng C, Li M, Chen R, Sugiura N (2011) Investigations on the batch and fixed-bed column performance of fluoride adsorption by Kanuma mud. *Desalination* 268(1–3):76–82
- Chiang HL, Chiang P (2000) Physicochemical characteristics of ozonation activated carbon. In: *Adsorption science and technology: proceedings of the second Pacific Basin conference on adsorption science and technology*. World Scientific, Warriewood, pp 135–139
- Choudhary M, Kumar R, Neogi S (2020) Activated biochar derived from *Opuntia ficus-indica* for the efficient adsorption of malachite green dye, Cu²⁺ and Ni²⁺ from water. *J Hazard Mater* 392. <https://doi.org/10.1016/j.jhazmat.2020.122441>
- Chowdhury S, Mishra R, Saha P, Kushwaha P (2011) Adsorption thermodynamics, kinetics and Isosteric heat of adsorption of malachite green onto chemically modified Rice husk. *Desalination* 265(1):159–168
- Clark RM (1987) Evaluating the cost and performance of field-scale granular activated carbon systems. *Environ Sci Technol* 21(6):573–580
- Chrihi A, Chlendi M (2011) Modeling of fixed-bed adsorption: application to the adsorption of an organic dye. *Asian J Text* 1: 161–171
- Das P, Das P, Datta S (2016) Continuous biosorption of malachite green by *Ananas comosus* (pineapple) leaf powder in a fixed-bed reactor: experimental, breakthrough time and mathematical modeling. *Desalin Water Treat* 57(53):25842–25847
- Dichiaro AB, Weinstein SJ, Rogers RE (2015) On the choice of batch or fixed-bed adsorption processes for wastewater treatment. *Ind Eng Chem Res* 54(34):8579–8586
- Ferreira CI, Calisto V, Otero M, Nadais H, Esteves VI (2017) Fixed-bed adsorption of Tricaine Methanesulfonate onto pyrolysed paper mill sludge. *Aquac Eng* 77:53–60
- Foo KY, Lee LK, Hameed BH (2013) Preparation of tamarind fruit seed activated carbon by microwave heating for the adsorptive treatment of landfill leachate: a laboratory column evaluation. *Bioresour Technol* 133:599–605
- Geçgel Ü, Üner O, Gökara G, Bayrak Y (2016) Adsorption of cationic dyes on activated carbon obtained from waste *Elaeagnus* stone. *Adsorpt Sci Technol* 34(9–10):512–525
- Goertzen SL, Thériault KD, Oickle AM, Tarasuk AC, Andreas HA (2010) Standardization of the Boehm titration. Part I. CO₂ expulsion and endpoint determination. *Carbon* 48(4):1252–1261
- Gopal N, Asaithambi M, Sivakumar P, Sivakumar V (2016) Continuous fixed-bed adsorption studies of Rhodamine-B dye using polymer bound adsorbent. *Indian J Chem Technol* 23:53–58
- Gouranchat, C. (2000). *Malachite Green in Fish Culture (State of the Art and Perspectives). Bibliographic Studies*. Nantes, France: École Nationale Vétérinaire de Toulouse (ENVT)
- Hameed BH, El-Khaiary MI (2008) Equilibrium, kinetics and mechanism of malachite green adsorption on activated carbon prepared from bamboo by K₂CO₃ activation and subsequent gasification with CO₂. *J Hazard Mater* 157(2–3):344–351
- Jerold M, Joseph D, Patra N, Sivasubramanian V (2016) Fixed-bed column studies for the removal of hazardous malachite green dye from aqueous solution using novel nano zerovalent iron algal biocomposite. *Nanotechnol Environ Eng* 1(1):8–17
- Kan Y, Yue Q, Kong J, Gao B, Li Q (2015) The application of activated carbon produced from waste printed circuit boards (PCBs) by H₃PO₄ and steam activation for the removal of malachite green. *Chem Eng J* 260:541–549
- Li Y, Zhang X, Yang R, Li G, Hu C (2015) The role of H₃PO₄ in the preparation of activated carbon from NaOH-treated rice husk residue. *RSC Adv* 5(41):32626–32636
- Liu D, Sun D (2011) Simulation of indigo carmine dye adsorption on polymer doped sawdust in fixed-bed systems. *Desalin Water Treat* 27(1–3):285–293
- Markovska L, Meshko V, Noveski V (2001) Adsorption of basic dyes in a fixed-bed column. *Korean J Chem Eng* 18(2):190–195
- Medvidović NV, Perić J, Trgo M (2008) Testing of breakthrough curves for removal of lead ions from aqueous solutions by natural zeolite-clinoptilolite according to the Clark kinetic equation. *Sep Sci Technol* 43(4):944–959
- Mohammadi M, Hassani AJ, Mohamed AR, Najafpour GD (2010) Removal of rhodamine B from aqueous solution using palm shell-based activated carbon: adsorption and kinetic studies. *J Chem Eng Data* 55(12):5777–5785
- Naja G, Volesky B (2006) Behavior of the mass transfer zone in a biosorption column. *Environ Sci Technol* 40(12):3996–4003
- Nouri H, Ouederni A (2013) Modeling of the dynamics adsorption of phenol from an aqueous solution on activated carbon produced from olive stones. *Int J Chem Eng Appl* 4(4):254–261

37. Oickle AM, Goertzen SL, Hopper KR, Abdalla YO, Andreas HA (2010) Standardization of the Boehm titration: part II. Method of agitation, effect of filtering and dilute titrant. *Carbon* 48(12):3313–3322
38. Pal P (2017) *Industrial water treatment process technology*. Butterworth-Heinemann, Oxford
39. Patel H, Vashi RT (2012) Fixed-bed column adsorption of ACID yellow 17 dye onto tamarind seed powder. *Can J Chem Eng* 90(1): 180–185
40. Prahaz D, Kartika Y, Indraswati N, Ismadji S (2008) Activated carbon from jackfruit peel waste by H_3PO_4 chemical activation: pore structure and surface chemistry characterization. *Chem Eng J* 140:32–42
41. Puttamat S, Pavarajam V (2016) Adsorption study for removal of Mn (II) ion in aqueous solution by hydrated ferric (III) oxides. *Int J Chem Eng Appl* 7(4):239–243
42. Redlich OJDL, Peterson DL (1959) A useful adsorption isotherm. *J Phys Chem* 63(6):1024–1026
43. Rocha PD, Franca AS, Oliveira LS (2015) Batch and column studies of phenol adsorption by an activated carbon based on acid treatment of corn cobs. *Int J Eng Technol* 7(6):459–464
44. Saadi Z, Saadi R, Fazaeli R (2013) Fixed-bed adsorption dynamics of Pb (II) adsorption from aqueous solution using nanostructured γ -alumina. *J Nanostruct Chem* 3(1):48–55
45. Singh SK, Townsend TG, Mazyck D, Boyer TH (2012) Equilibrium and intra-particle diffusion of stabilized landfill leachate onto micro-and meso-porous activated carbon. *Water Res* 46(2):491–499
46. Sun X, Imai T, Sekine M, Higuchi T, Yamamoto K, Kanno A, Nakazono S (2014) Adsorption of phosphate using calcined Mg3–Fe layered double hydroxides in a fixed-bed column study. *J Ind Eng Chem* 20(5):3623–3630
47. Tan IAW, Ahmad AL, Hameed BH (2008) Adsorption of basic dye using activated carbon prepared from oil palm shell: batch and fixed-bed studies. *Desalination* 225(1–3):13–28
48. Tang SH, Zaini MAA (2017) Malachite green adsorption by potassium salts-activated carbons derived from textile sludge: equilibrium, kinetics and thermodynamics studies. *Asia Pac J Chem Eng* 12(1):159–172
49. Tang SH, Zaini MAA (2020) Development of activated carbon pellets using a facile low-cost binder for effective malachite green dye removal. *J Clean Prod* 253. <https://doi.org/10.1016/j.jclepro.2020.119970>
50. Thomas HC (1944) Heterogeneous ion exchange in a flowing system. *J Am Chem Soc* 66(10):1664–1666
51. Van der Bruggen B, Schaep J, Wilms D, Vandecasteele C (1999) Influence of molecular size, polarity and charge on the retention of organic molecules by nanofiltration. *J Membr Sci* 156(1):29–41
52. Vijayalakshmi G, Sivajiganesan S (2020) Removal of malachite green dye by teak wood waste biomass activated carbon and its antimicrobial activity. *Eur J Med Plants* 31(6):18–25
53. Wang J, Kaskel S (2012) KOH activation of carbon-based materials for energy storage. *J Mater Chem* 22(45):23710–23725
54. Wang YH, Lin SH, Juang RS (2003) Removal of heavy metal ions from aqueous solutions using various low-cost adsorbents. *J Hazard Mater* 102(2):291–302
55. Wu FC, Liu BL, Wu KT, Tseng RL (2010) A new linear form analysis of Redlich–Peterson isotherm equation for the adsorptions of dyes. *Chem Eng J* 162(1):21–27
56. Xu Z, Cai JG, Pan BC (2013) Mathematically modeling fixed-bed adsorption in aqueous systems. *J Zhejiang Univ Sci A* 14(3):155–176
57. Yagub MT, Sen TK, Afroze S, Ang HM (2015) Fixed-bed dynamic column adsorption study of methylene blue (MB) onto pine cone. *Desalin Water Treat* 55(4):1026–1039
58. Yoon YH, Nelson JH (1984) Application of gas adsorption kinetics I. theoretical model for respirator cartridge service life. *Am Ind Hyg Assoc J* 45(8):509–516

Publisher's Note Springer Nature remains neutral with regard to jurisdictional claims in published maps and institutional affiliations.